The application of roughness model to a soft EHL contact

M.F.J. Bohan, T.C. Claypole and D.T. Gethin
Department of Mechanical Engineering, University of Wales, Swansea

Keywords *Surface roughness, Fluid flow, Lubrication*

Abstract *The study focuses on the development of a numerical model to explore the impact of surface roughness in soft rolling nip contacts, including representation of a real surface. The solution of the governing equations required the application of a multigridding technique to capture the details of the fluid flow within the roughness wavelengths and a minimum number of fluid nodes per wavelength were established. In the case studies, two extreme roughness profiles were considered, longitudinal and circumferential. The longitudinal roughness had a significant impact on nip pressures and pumping capacity, the latter being determined by the minimum film thickness in the nip. The circumferential roughness was found to have a localised effect on film pressure, but only a very small impact on the film thickness profile. The consequent effect on pumping capacity was small.*

Nomenclature

a = Hertzian contact width
b_k = body forces within boundary domain
c^i_{lk} = corner factor for the boundary integral equation
E^* = equivalent elastic modulus
g = fundamental solution of Reynolds equation
h = fluid film thickness
L = load
p = fluid pressure
p_k = traction for the boundary integral equation
p^*_{lk} = traction for Kelvin solution
p_n = fluid pressure at point x_n
R = equivalent roller radius
r_a = roughness amplitude
r_f = roughness frequency
r_p = roughness phase
U = mean sum of the roller surface velocities
u = surface indentation
u_k = displacement for the boundary integral equation
u^*_{lk} = displacement for Kelvin solution
v_n = pressure gradient dp/dx at point x_n
x = co-ordinate for film
Γ = boundary surface
δ = Dirac delta function
ζ = point on the boundary
μ = fluid viscosity
ψ = term within the Reynolds equation
Ω = boundary domain

Introduction

The transfer of a fluid to a substrate in a controlled manner is used in many industrial applications. This is often achieved by the use of alternate hard and rubber covered rollers, Figure 1 and these will operate under conditions ranging from pure rolling to pure sliding dependent on the process. In certain instances a simultaneous lateral motion of the rollers is also employed. In many designs, the systems are used with positive engagements, imposing the

International Journal of Numerical Methods for Heat & Fluid Flow, Vol. 12 No. 4, 2002, pp. 356-374.

DOI 10.1108/09615530210433260

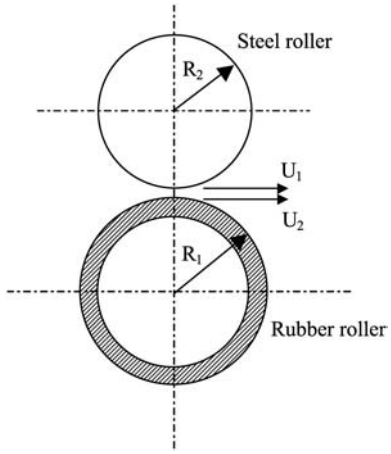

Figure 1.
Schematic of a roller contact

requirement to use a roller covered with a soft rubber and the consequent pressures generated in the nip contact result in significant rubber deformations.

Pressure is generated in the nip by mechanical deformation and hydrodynamic action as the fluid is entrained through the contact. This pressure field developed by this combined action will lead to the deformation of the elastomeric layer and this deformation will affect the film thickness and hence the hydrodynamic pressure component in the nip contact. This contact is referred to as that of Soft Elasto Hydrodynamic Lubrication (Soft EHL) and since the rollers are usually long in comparison with diameter and especially the contact geometry, this effectively forms a line contact.

The emphasis in this paper is concerned with roughness effects in soft EHL contacts, however it is appropriate to review briefly previous work on smooth contacts and this will be dealt with initially. The experimental and numerical analyses of nips have been reported on extensively in the literature. Initial work on dry contacts (Hannah, 1951) has formed the basis of much of this analysis. The methods have been expanded to evaluate boundary conditions (Miller, 1966) and the roller parameters (Meijer, 1968; Jaffar, 1993). The lubrication of layered contacts was first explored in the field of journal bearings (Higgson, 1965–1966) and this was later generalised to contacts with different surfaces in which only small deformations were present (Bennett and Higginson, 1970). The general treatment of large deformation is counterformal contacts is discussed in Hooke and O'Donoghue, 1972. It is assumed that pressure in the nip is dominated by a Hertzian component and separate functions are used to describe the inlet and outlet regions. This was later extended to layered solids (Gupta, 1976), including developments to accommodate a Poissons ratio of 0.5 that is appropriate for rubber and normally introduces a singularity into the

governing elasticity equations. The model was used to explore a wide range of loading conditions.

In many of the preceding works, the linkage between deformation and hydrodynamic action was excluded since the contacts were either dry, or heavily loaded with emphasis on transmissions or rolling element bearing application. The necessity to iterate between the fluid and structural domains was first highlighted in Cudworth, 1979 with specific emphasis on a soft EHL analysis. This has since been developed to evaluate different modes of lubrication dependent on the nip conditions (Hooke, 1986). These have then been further extended to different inlet and process conditions for Newtonian (MacPhee *et al.*, 1992; Bohan *et al.*, 1997) and non-Newtonian fluids (Lim *et al.*, 1996).

All the work reviewed above assumes that the roller surfaces are smooth. One of the first approaches to modelling rough lubricated contacts is set out in Patir and Cheng, 1978 where the authors describe a model where flow coefficients are introduced into the Reynolds equation to capture both isotropic and anisotropic surfaces, idealised using a Gaussian distribution and incorporating anisotropy via a length scale. This approach is particularly applicable in hydrodynamic lubrication, or under circumstances where piezoviscous fluids are not used and the usual pressure term in the Reynolds equation is still significant. Some controversy surrounds the determination of the coefficients that capture the surface geometry, particularly where the film thickness gradients associated with asperities are steep. This has received attention recently in Lunde and Tønder, 1997 in which the authors examine a patch within a bearing film, but use the Reynolds equation to approximate the flow. Subject to the local application of the Reynolds equation, this allowed a calculation of pressure fluctuation details in response to the local asperity profile and the distribution was superimposed on an average pressure generated from the mean film profile.

Surface roughness studies in contacts between hard counter-formal surfaces has focused on nips lubricated by fluids that exhibit a strong piezoviscous behaviour and this has been coupled with elastic deformation of the contact. The consequent high viscosity in the denominator of the pressure term in the Reynolds equation effectively removes this term from the equation. This modelling approach has been explored vigorously recently, mainly in connection with gear and rolling element contacts (Hooke, 1999; Greenwood, 1999). These studies develop models focusing on transport of roughness through the contact, leading to pressure waves and roughness waves of different frequency moving through the contact under circumstances of sliding motion. Under conditions of rolling motion, the original roughness profile is retained and the pressure profile reflects the local film thickness variations.

An up to date review of work in hard elastohydrodynamic lubrication is set out in Dowson and Ehret, 1999 in which the authors have critically examined

key studies chronicling the developments in this area, culminating in work on real surfaces and real lubricants. The present study also addresses this topic, but with specific application to soft elastohydrodynamic contacts in which the deformations are large and the viscosity remains low. Therefore the roughness transport models are not appropriate and the film model will need to account for pressure terms as well as the surface topography.

The purpose of this paper is to evaluate high frequency roughness profiles in a computationally efficient manner. It will to explore the effect of both circumferential and longitudinal roughness profiles on the roller. The applicability of the idealised sinusoidal roughness as an approximation to the real roughness profiles will also be assessed.

Theoretical model background

The overall solution of the soft elastohydrodynamic lubrication problem that is generic to many printing and coating applications is obtained by coupling the solutions from the Reynolds equation with that of the elastic deformation of the roller. Following the review of previous work, this requires a procedure that iterates between the solutions for the structural and fluid domains. Of particular importance to this study is the background theory for solution, with the introduction of roughness characteristics. This will be discussed, followed by its incorporation into the solution procedure.

Reynolds equation

For a Newtonian fluid and a thin film the Reynolds equation may be used to describe the hydrodynamic behaviour in the nip (Dowson, 1962). Provided that the contact width is small in comparison with the roller diameter and the analysis plane is some distance from the roller edge then the Reynolds equation can be written in a one-dimensional form as

$$\frac{d}{dx}\left[\frac{h^3}{12\mu}\frac{dp}{dx}\right] = \left(\frac{u_1 + u_2}{2}\right)\frac{dh}{dx} \tag{1}$$

The assumption of a Newtonian fluid is retained in this work and this is shared with many other publications (MacPhee *et al.*, 1992; Bohan *et al.*, 1997). Some printing inks are non-Newtonian and this can affect the flow characteristics (Lim *et al.*, 1996), however this will be described in a separate investigation. In this solution, the pressure at the inlet and outlet were set to zero together with the pressure gradient, satisfying a well-established Swift-Steiber condition. This was set automatically within the code and it effectively determines the rupture point in the contact to ensure flow continuity. However this condition ignores the possible occurrence of sub-ambient pressures (Lim *et al.*, 1996) that may be treated using an approach balancing viscous and surface tension forces (Carvalho and Scriven, 1997). The choice of the simpler Swift-Steiber condition is justified at this point since this work focuses on the inclusion of roughness

effects, treatment of different film boundary conditions in association with roughness effects will require further detailed attention.

For the purpose of computational efficiency, the Reynolds equation was solved using Green's function with the right hand side of equation (1) replaced by the Dirac delta function $\delta(x-\zeta)$. The solution can be obtained using the following for $g(x,\zeta)$ and its differential, where $h^* = h^3$.

$$g(x,\zeta) = \begin{cases} \int_{\zeta}^{x} \frac{1}{2h^*} dx \ \ for\, \zeta > x \\ -\int_{\zeta}^{x} \frac{1}{2h^*} dx \ \ for\, \zeta < x \end{cases}, \quad \frac{dg(x,\zeta)}{dx} = \begin{cases} \frac{1}{2h^*} \ \ for\, \zeta > x \\ -\frac{1}{2h^*} \ \ for\, \zeta < x \end{cases} \tag{2}$$

Using equation (2) and the Dirac function, the Reynolds equation (1) can be solved providing the following expression for the pressure

$$\begin{aligned} p(\zeta) = {} & [-h^*(x_1)g(x_1,\zeta), h^*(x_2)g(x_2,\zeta)] \begin{bmatrix} v_1 \\ v_2 \end{bmatrix} \\ & + \left[h^*(x_1)\frac{dg}{dx}\Big|_{x=x_1}, -h^*(x_2)\frac{dg}{dx}\Big|_{x=x_2} \right] \begin{bmatrix} p_1 \\ p_2 \end{bmatrix} + \int_{x_1}^{x_2} \psi(x) \cdot g(x,\zeta) dx \end{aligned} \tag{3}$$

Elasticity equations

A number of schemes are available for solving the elasticity equations in the rubber layer. Since deformation is the main focus in this application, this is achieved most economically using a boundary element approach. Assuming the rubber layer on the roller to be linearly elastic due to the relatively small deformation in comparison with its thickness, for a plain strain case, the boundary element integral equation for the solution of the general problem of elastostatics is given below (Brebbia and Dominguez, 1989).

$$c^i_{lk} u^i_k + \int_{\Gamma} p^*_{lk} u_k \, d\Gamma = \int_{\Gamma} u^*_{lk} p_k \, d\Gamma + \int_{\Omega} u^*_{lk} b_k \, d\Omega \tag{4}$$

However, for the problem examined, the body forces are zero, with no thermal or gravitational forces and the equation can be simplified to

$$c^i_{lk} u^i_k + \int_{\Gamma} p^*_{lk} u_k \, d\Gamma = \int_{\Gamma} u^*_{lk} p_k \, d\Gamma \tag{5}$$

This equation can be formulated as a matrix and solved readily for the displacement of the rubber layer. The integrals of the elasticity equation were calculated over the boundary and represented by the sum of integrals over each

of the boundary elements. The element integrals were calculated analytically to ensure computational efficiency. In the model, compatible with the assumption for the film, the elastomer was unwrapped as shown in Figure 2. The lower surface was constrained rigidly to represent adhesion between the steel core and rubber cover and no circumferential movement was allowed at the lateral extremes of the calculation domain.

Film thickness equation

The film thickness is defined by equation (6). The roller roughness is incorporated into this together with the deformation due to the roller loads and a negative value of h_0 represents roller engagement.

$$h(x) = h_0 + \frac{x^2}{2R} + u(x) + r(x) \tag{6}$$

In equation (6), $r(x)$ is the roughness applied to the surface of the roller. This can be defined either as a regular roughness profile or actual measured data can be incorporated as a function of distance through the nip. Within the paper both methods have been employed and their impact investigated. When treated as a function, the roughness profile is given by the equation

$$r(x) = \frac{r_a}{2} \cdot \sin(r_f(x) + r_b) \tag{7}$$

For the actual roughness data a look up table has been generated at the correct nodal intervals based on experimentally measured surfaces and the roughness obtained from an array, given as

$$r(x) = r_m(x) \tag{8}$$

In utilising the approach set out above, it is assumed that the amplitude and wavelength of the roughness is not sufficient to generate localised reverse flows within the asperity zone itself (Lunde and Tønder, 1997). If this occurs, then it can only be dealt with accurately via solution of the Navier Stokes equations and this is computationally prohibitive at this time.

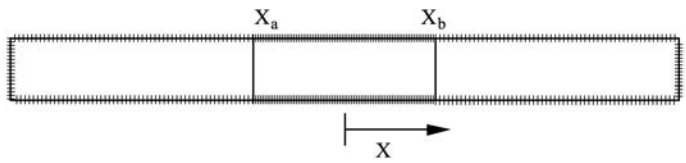

Figure 2.
Schematic discretisation of the boundary

Load

To reflect operation, the rollers are forced into engagement at a pre set level of load. This was embodied in the model and closure of the solution was obtained by the load meeting the following criterion

$$\int_{x_1}^{x_2} p \cdot dx = L \tag{9}$$

Solution procedure

Calculations have been carried out for a rolling nip contact since this is free from the additional complication of roughness and pressure waves travelling through the nip as discussed in Hooke, 1999; Greenwood, 1999. Where sliding is present, coupled with longitudinal roughness, the asperity on the rubber roller surface is likely to be deformed and it will tend to a smoother surface, however this is excluded from the current investigation. However, prior to this investigation, the local deformation of the roughness profile when subjected to a pure pressure loading was analysed using commercial finite element analysis software. The roughness profile was entered as a sinusoidal function based on data obtained from white light interferometry measurements of actual surface roughness profiles from which indications of wavelength and amplitude were derived. Pressure levels were used from experimental data on smooth rollers (Lim *et al.*, 1996) and the material properties of the rubber were determined experimentally. The variables investigated using this system were the mean rubber thickness, pressure, roughness amplitude and the roughness frequency.

In all the models, load was applied to the waveform surface such that the pressure was normal to the rubber surface. For the section considered, the sides of the rubber were constrained in only the X direction allowing for compression, while the base was fixed in both X and Y as they are bonded to a metal core.

Typical displacements computed suggest a change in the profile of 0.5 μm for a roughness depth of 50 μm, the maximum percentage change in the profile height for all the model cases was 1 per cent, essentially capturing the near incompressible rubber property. The analysis shows that for the rubber covering materials and surface profiles used within printing and roller coating applications in which there is a near pure rolling action, the use of a fixed roughness profile is applicable. For further details refer to Bohan *et al.*, 2001.

Compatible with the derivation set out above, within the current approximation an equivalent radius approach was used and the elastomer was unwrapped as shown in Figure 2 where the boundary of the elastomer is subdivided into a number of elements. The equivalent radius approach is appropriate for narrow contact widths and has been shown not to significantly affect the results (Dowson and Higginson, 1959). From the elastomer mesh the fluid domain is applied over the nip contact, $X\mathrm{s}_\mathrm{a}$ to X_b. Since this is sufficiently

remote from the extreme ends of the elastomer, this will eliminate the effect of structural boundary conditions on the simulation of this local fluid structure interaction.

Numerical singularities can occur when a field point ζ_0 is located at a node where the integration takes place. These can be eliminated with the use of corner factors and the techniques are indicated in Brebbia and Dominguez, 1989; Banerjee and Butterfield, 1981.

Consistent with the elastomer mesh, the fluid domain was solved over the nip contact, X_a to X_b. Since this solution strategy accounts for roughness directly by modification of the film thickness profile, the Reynolds equation was solved within the scale of the roughness profile. The interaction with the elastomer was then applied directly via local integration of the pressure field and assigning the resultant force to the adjacent node on the elastomer surface. This may include the data from multiple roughness wavelengths, Figure 3. To achieve an accurate solution, the divisions for the pressure equation solution must be appropriate for the roughness profile wavelength. This effectively leads to a multi grid solution strategy and the sensitivity with respect to this strategy will be explored within the initial numerical studies.

The solution of soft EHL contacts is particularly troublesome due to the large deformation of the elastomer in response to the pressure field and this can lead to large and diverging oscillation (Lim *et al.*, 1996). Following extensive previous development a stable strategy to handle this coupled system has been established as

(1) Assign mesh division and calculate the roughness frequency; recalculate the mesh division if the required nodal sub division is not appropriate.

(2) Set an initial value for the engagement, h_0, from this the Hertzian pressure and the consequent deformation is calculated.

(3) Calculate the film thickness in the nip junction.

(4) Calculate the film pressure.

(5) Recalculate the deformation.

(6) If the deformation has not met the convergence criterion, then repeat from stage (3) with the new deformation.

(7) Once the deformation criterion has been met, examine the load equilibrium. If this is not met then appoint a new value for h_0 and repeat from (2).

The convergence requirement for the analysis was set to be 0.1 per cent on the pressure and indentation, with a minimum number of elements within the roughness wavelength being 36. Overall solution convergence was generally obtained within 500 iterations.

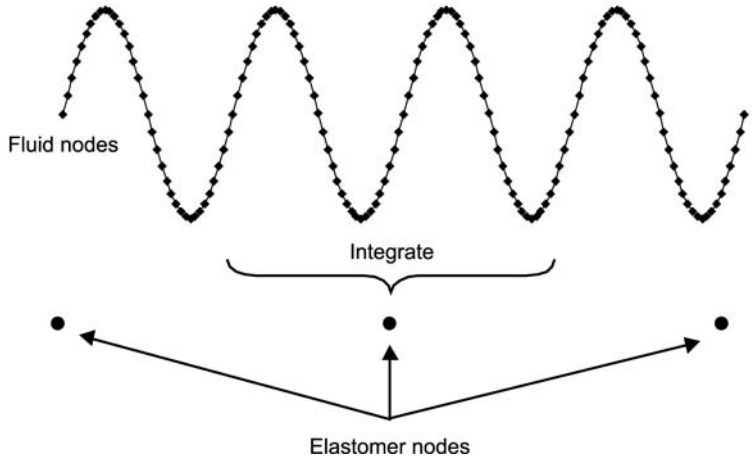

Figure 3.
Discretisation of the fluid regime and connectivity to the elastomer nodes

Sensitivity of surface parameters on the behaviour in the nip

For the purposes of the analysis, a typical industrial printing configuration was chosen and the relevant details are, shown in Table I. They relate to press geometry and the material parameters and guidance on roughness parameters has been derived from measurements. These have been used to show the influence of roller surface roughness on the pressure profile, film thickness and fluid flow rate through the nip. The latter is a main concern in printing and coating application and this is in contrast with hard nip contacts where pressure and film thickness is the focus of attention.

Roughness on the roller surface can be described in extreme circumstances as either longitudinal or circumferential. These are shown in Figure 4 with the longitudinal roughness (a) representing areas of roughness along the roller axis while the circumferential roughness (b) represents the roughness peaks going around the roller. The two types of roughness appear in different applications, dependent on the machine finish applied to the roller. When treating roughness effects directly it is convenient to represent the effect of roughness in both

Parameter	Conditions
Load (Nm^{-1})	1750
Roller speed (ms^{-1})	0.25
Fluid viscosity (Pa.s)	3.0
Roller radius (m)	0.045
Rubber layer elastic modulus (Pa)	4.0e+6
Rubber thickness (mm)	8
Rubber roller roughness amplitude (μm)	50
Rubber roller roughness frequency (μm)	50

Table I.
Process parameters used in the sensitivity study

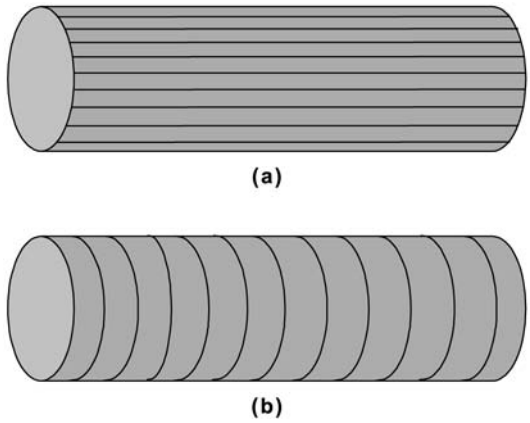

Figure 4.
Schematic of roughness models

directions by combining the solution routines for both the longitudinal or circumferential analysis. A more formal treatment will require a two-dimensional application of the Reynolds equation (Lunde and Tønder, 1997) and when coupled with a deformation analysis, this will again be computationally prohibitive.

Longitudinal roughness

Initially a sensitivity analysis was carried out to evaluate the number of nodes required within each roughness wavelength. The consistency of the results on the pressure, film thickness and flow were evaluated and the results from the flow analysis are shown in Figure 5. The flow was used since this combines both the pressure and film thickness and was the most sensitive parameter with which to optimise the nodal frequency. This work showed that the minimum number of fluid elements within a roughness wavelength should be 36 to obtain a reliable result as well as enforcing local mass conservation. This was used for all subsequent analysis.

The pressure distribution throughout the nip contact shows significant effects for changes in the roughness wavelength, Figure 6, with the effects increasing through the contact. As the wavelength of the roughness increases, noticeable pressure fluctuations are set up in the contact and progressively larger pressure perturbations are predicted. In addition, these increased perturbations lead to some change in the rupture point at the outlet from the contact, particularly at the longer wavelength.

Recent work (Hooke, 1999), primarily on hard narrow contacts, has focussed on relatively long wavelengths, leading to only 5 to 10 complete wavelengths through the contact. The results in Figure 6 show that the profiles obtained under these conditions may not be representative of those found in many

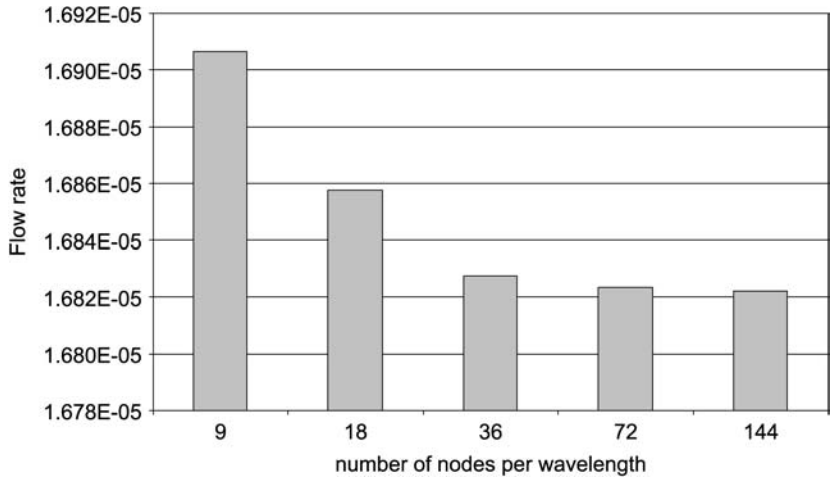

Figure 5.
Multi-griding sensitivity

printing applications where the wavelength of the roughness is much smaller and the contact is significantly wider.

The main purpose of the analysis is to focus on the nip pumping capacity that combines both pressure gradient and film thickness components. Although the roughness profile has an impact on the pressure profile, it may be more appropriate to present averaged (or smoothed) profiles, particularly where the roughness wavelength is short. Thus to aid interpretation of the influence of roughness on the performance through the nip, the pressure and film thickness profiles have had a smoothing function applied. In the analysis,

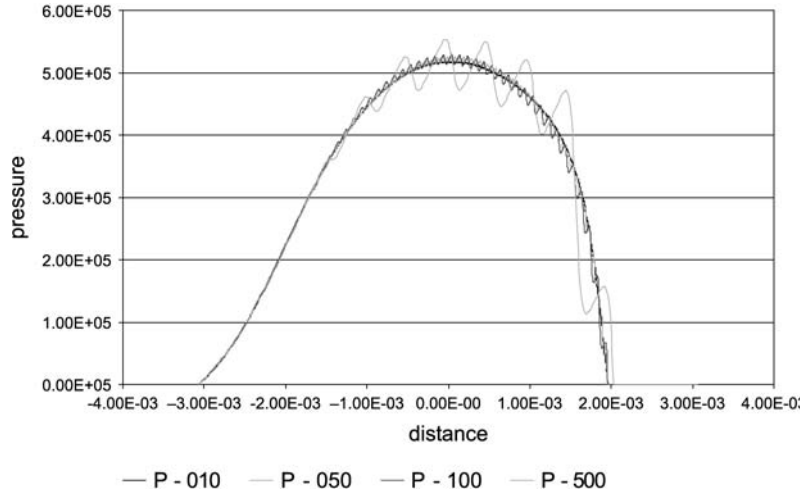

Figure 6.
Pressure distribution for changing wavelength: mean roughness amplitude 50 μm

smoothing combines all the data over a single wavelength and provides an average pressure or film thickness at the mean x co-ordinate of the data that has been analysed.

The roughness amplitude has a large effect on the film thickness profile, Figure 7. The pressure profiles were not modified substantially with only a small increase in maximum pressure, less than 1 per cent. The profiles clearly reflect the constant level of load application demonstrating no marked deviations. In contrast, as the roughness increases the mean film thickness increases, but maintains a consistent form. However, analysis of the actual (non smoothed) film thickness profiles showed that while the mean thickness increases, the minimum gap through the contact decreases. The consequent impact on flow through the nip will be highlighted below.

The impact of changes in the roughness wavelength and phase have also been explored (Bohan *et al.*, 2001). These parameters induce only small changes to both the mean pressure and film thickness profiles, the largest differences are apparent for the maximum pressure encountered in the nip contact. The averaging for the longer wavelengths showed quantization errors due to the length of the cycle compared to the overall nip contact.

The changes of flow rate with the roughness parameters are shown in Figure 8 where clearly roughness amplitude has the most dramatic impact through reduction in flow. This is contrary to what may be expected based on

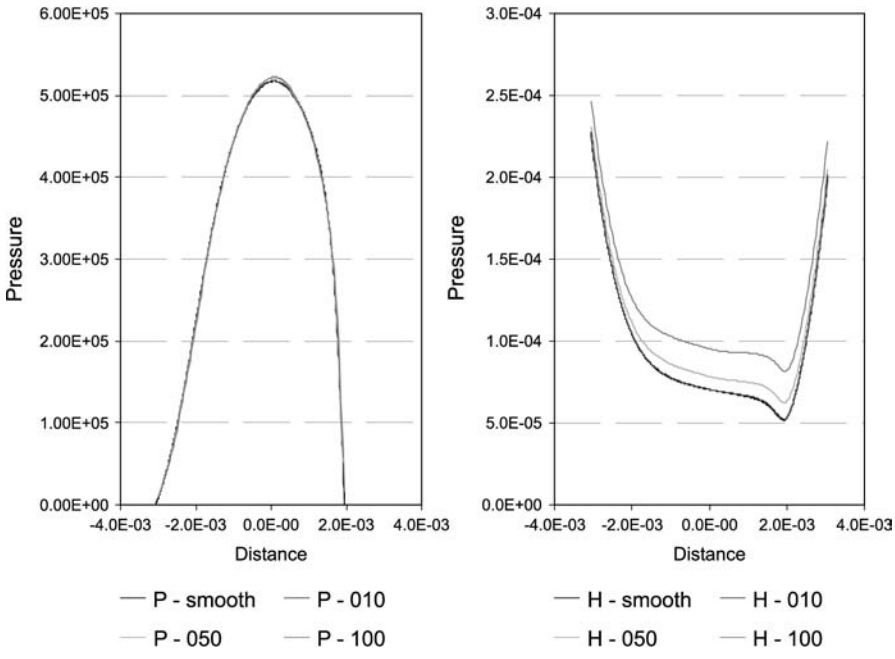

Figure 7.
Pressure and film thickness variations with roughness amplitude

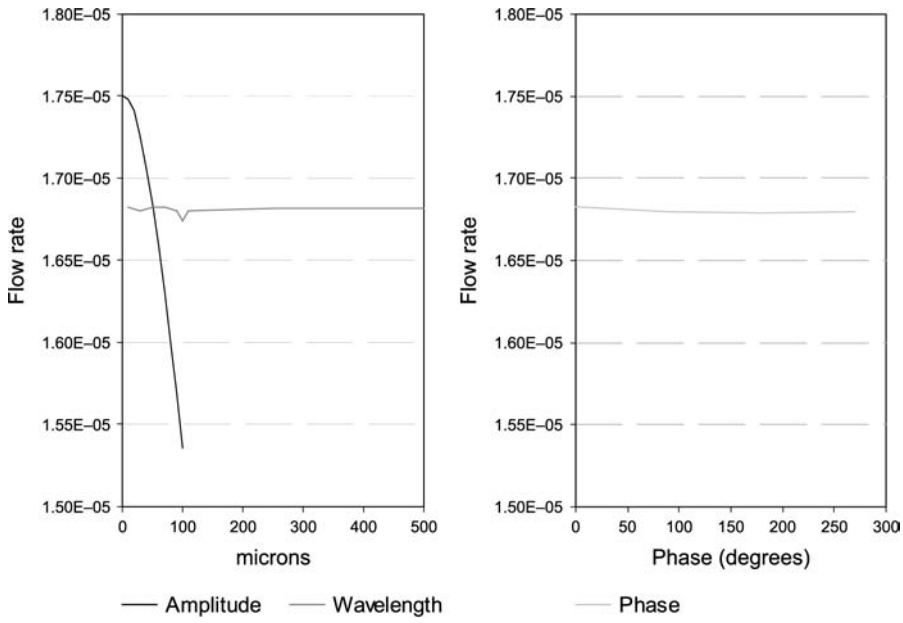

Figure 8.
Flow rate changes with roughness amplitude

the average film thickness that increases with roughness, whereas the minimum film thickness reduces. This confirms that the minimum film thickness determined by the nominal thickness and roughness in the contact determines the pumping capacity. These result compare directly and favourably with the trends for transverse roughness presented in Patir and Cheng, 1978 where the flow factor drops off as the ratio of roughness amplitude to mean film thickness increases. The remaining parameters of wavelength and phase have negligible impact on the pumping capacity within the nip.

Circumferential roughness

Using a direct modelling approach, the treatment of circumferential roughness as shown schematically in Figure 4 is not straight forward. In this work, it has been tackled by dividing the roller into slices through the diameter and solving the governing equations of Soft EHL on the slice. Two extreme scenarios exist, where there is positive clearance in which hydrodynamic deformation is neglected, and where there is complete engagement. Where a clearance gap exists, this infers the neglect of any lateral flow and combining solutions having different minimum film thickness, dependent on the surface profile and slice location. For the loaded condition, the film thickness is determined from the nip analysis modified according to the roughness amplitude. The behaviour has been explored for the case of the sinusoidal profile shown in Figure 9 and the physical parameter settings defined in Table I. For these extreme cases, the

nip width will vary relative to the film thickness, representing flooding for a thin film and starvation in the case of a thick gap. The choice of an appropriate setting is therefore not straightforward and strictly requires a mass balance on the flow entering the nip coupled with its impact on pumping capacity to estimate a formation position. This requires a two dimensional representation of the film that is outside the scope of the present analysis and therefore contact width will need to be estimated as an input variable to the analysis.

Numerical models evaluating the nip performance for a pair of rigid rollers in close contact was carried out. This sensitivity of the system for the roller gap between 1 and 10 microns showed the flow was dominated by the Couette component and minimum film thickness, the gap between the two rollers. The degree of starvation of the contact (prescribed by the contact width) was found to have minimal effects on the flow through the nip.

For the case of engagement, initial calculation was performed for a smooth surface. This gave an engagement (h_0) of 250 μm and this has been used as the datum. Altering this by the roughness amplitude then simulates the surface roughness effect. This necessitates a change in the solution sequence presented above, with the load being the variable altered while the engagement is now fixed.

For a change of 50 μm engagement, the most significant changes occur in the pressure profile and the consequent film width, Figure 10. As the engagement is reduced the contact width reduces and the maximum pressure in the nip also reduces. However, there is much less impact on the final film thickness in the nip, even though the roughness amplitude is 20 per cent of the engagement. There are minor effects such as the point of minimum fluid film thickness moving forward towards the centre of the nip while also increasing, but only by a very small amount.

The results indicate that the circumferential roughness has a much greater impact on the pressure profile than the longitudinal roughness, although this result is likely to be mitigated if a two dimensional film analysis is applied. The most significant result is that the final film thickness profile is not affected significantly by roughness and the pressure profiles retain a similar form.

The impact of the different engagements on flow rate is shown in Figure 11. As expected, as the engagement between the two rollers is increased, the flow rate decreases and conversely. The most important result is that the overall

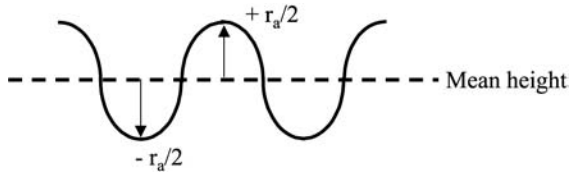

Figure 9.
Schematic of a rough roller surface

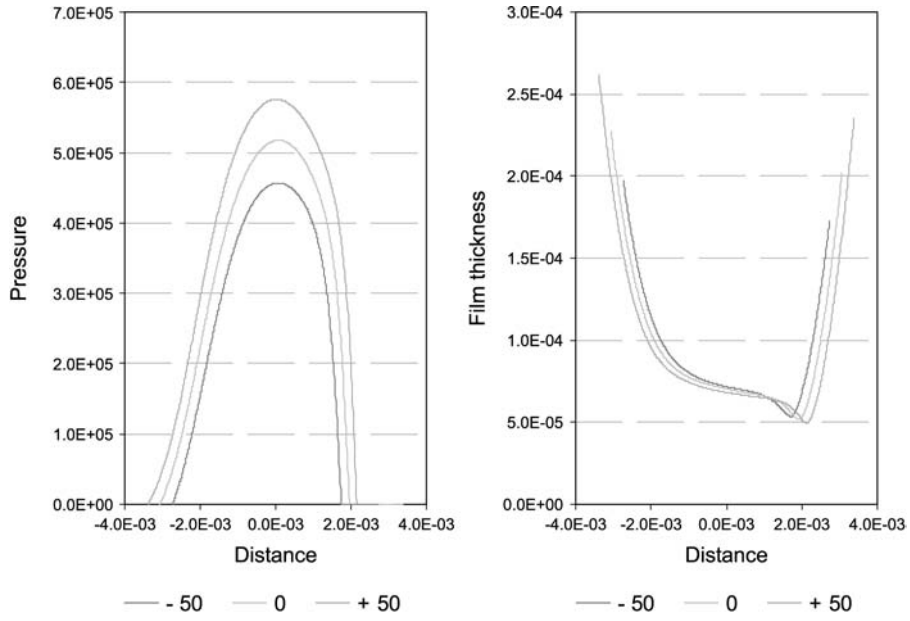

Figure 10.
Pressure and film thickness variations with varying nip gap

impact of circumferential roughness on nip pumping capacity is likely to be small. This is also supported by noting that the ratio of film thickness to roughness is typically 5 for which the effect on flow factor in the film is small (Patir and Cheng, 1978). This is particularly fortuitous since the rubber rollers are generally finish machined by grinding, giving a roughness profile that is

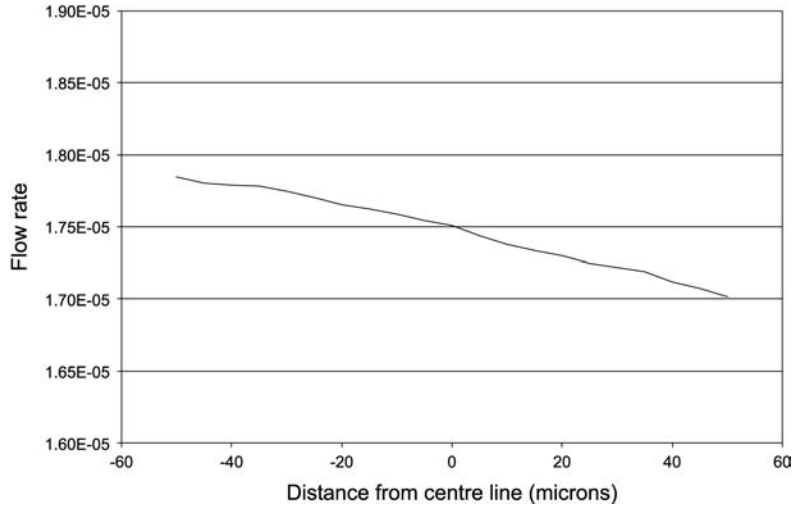

Figure 11.
Flow rate changes with varying nip gap

mainly circumferential. The result implies that achieving a fine surface finish in the circumferential direction may not be so important with respect to pumping capacity within the nip. In comparing longitudinal and circumferential roughness effects, the results indicate that there are significant differences for equal changes in roughness amplitude. Longitudinal roughness changes will affect the flow rate to a much greater extent, with more than double the reduction in pumping capacity in the nip.

Modelling actual roughness profiles

The roughness definition, equation (7), has been incorporated such that it can be replaced with an actual roughness profile recorded digitally from a roller surface. To illustrate this, the roughness of a typical surface was measured using white light interferometry, with a measurement area of 1 mm side dimension. This yields roughness data in both circumferential and longitudinal directions. According to Figure 5, the frequency of the roughness profile effectively defines the discretisation of the fluid domain. To capture the varying frequency of the local surface roughness requires a structural discretisation that adapts to the local roughness wavelength and where high frequency components are present this will lead to a very fine discretisation and consequently long computation times. In this analysis, a mask of wavelength of 50 μm was applied to the roughness profile and in accordance with Figure 5, this was divided into 36 increments, effectively dividing the trace into 1.36 μm increments. Digitising the surface trace gave the roughness profile displayed in Figure 12 and because the contact nip exceeds 1 mm, this profile group was then repeated six times over the contact width. On a local basis, the film gradients are large and these may have an impact on the flow within this

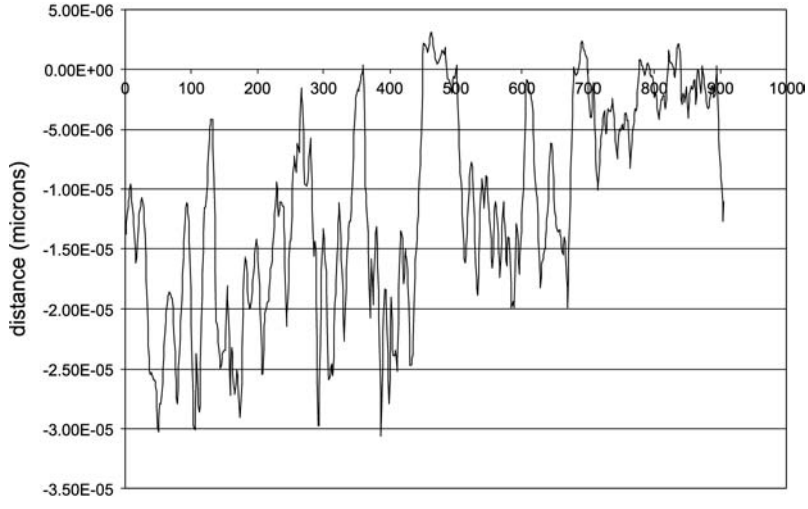

Figure 12.
An actual surface roughness profile

microscopic region (Lunde and Tønder, 1997). Strictly accurate simulation will require solution of the Navier Stokes equation within the region and it is beyond the capability of currently available computation to extend this over the contact width.

When subjected to a load of $1750\,\mathrm{Nm}^{-1}$ the consequent pressure and film thickness profiles are shown in Figure 13. In performing this analysis, no numerical stability difficulties were encountered. When compared with Figure 6 and Figure 7, the generic characteristics such as film width, pressure level and clearance profile remain closely similar. However, differences in detail are present, most specifically in the pressure profile where a smooth excursion to a maximum value is absent. The flow rate through the nip contact is reduced, by a similar amount to that calculated for the longitudinal roughness amplitude of 30 microns. This indicates that it is the total range of the roughness profile, "R_z" and not the "R_a" that is the key factor in relating the simplified sinusoidal roughness to the real roughness values.

Conclusions

A fast and computationally efficient model including roughness effects has been developed for a soft elastohydrodynamic contact lubricated using a Newtonian fluid. This is capable of assessing both axial and circumferential sinusoidal roughness profiles and it can also quantify the effects of real rough surfaces. The numerical analysis couples the solution of the Reynolds equation and those of the elastomer and incorporates the roughness profile directly within the film thickness profile in the Reynolds equation. A sensitivity study has been completed to establish the impact of roughness on the film thickness

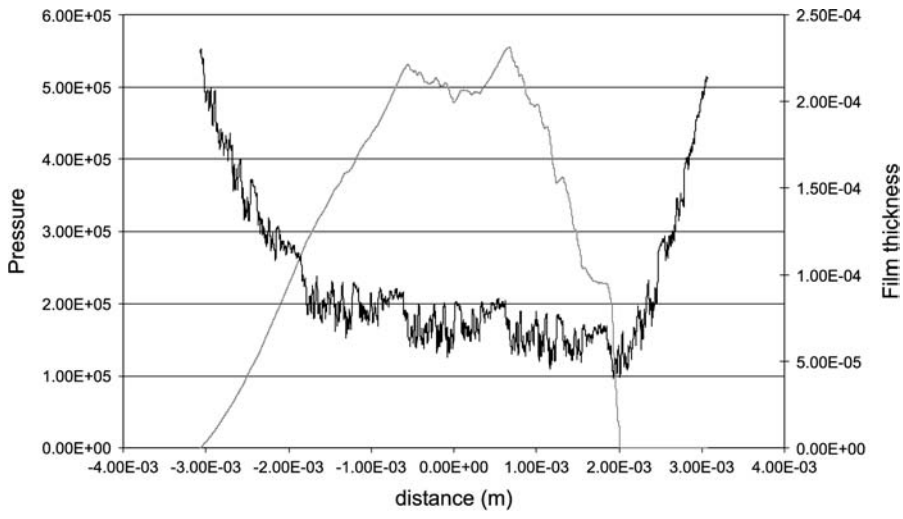

Figure 13.
Pressure and film thickness profiles for the actual roughness profile

and pumping capacity within the nip. The following conclusions can be drawn from this work.

- A multi gridding technique was found to work successfully, linking the hydrodynamic pressure to elastomer deformation and a sensitivity study confirmed that for a sinusoidal roughness profile, a minimum of 36 fluid nodes is required within each roughness wavelength.
- For longitudinal roughness and a fixed loading level, amplitude has the most significant impact on the mean film thickness. However, the flow rate through the nip is governed completely by the local minimum film thickness and not its averaged value. Therefore, increasing the roughness results in a significant decrease in the flow rate. Roughness wavelength only affects the pressure profile, with increased response at the longer wavelengths when waviness exists.
- The effect of circumferential roughness on final film thickness was found to be negligible and consequently had only a small impact on the pumping capacity within the nip.
- For a longitudinal roughness and the incorporation of real surface topography the generic form of the pressure and film thickness remain relatively unchanged, however on a local basis it has a most significant impact on the pressure that is generated within the nip.

References

Banerjee, P.K. and Butterfield, R. (1981), *Boundary element method in engineering science*, McGraw Hill, New York.

Bennett, J. and Higginson, G.R. (1970), "Hydrodynamic lubrication of soft solids", *Proc. I. Mech. E. Journal of Mechanical Engineering Sciences*, 12, pp. 218-22.

Brebbia, C.A. and Dominguez, J. (1989), *Boundary elements: An introductory course*, McGraw Hill.

Bohan, M.F.J., Lim, C.H., Korochkina, T.V., Claypole, T.C., Gethin, D.T. and Roylance, B.J. (1997), "An investigation of the hydrodynamic and mechanical behaviour of a soft nip in rolling contact", *Proc. I Mech E part J Engineering Tribology*, 211 No. J1, pp. 37-50.

Bohan, M.F.J., Claypole, T.C. and Gethin, D.T. (2001), *Roughness modelling of soft elastohydrodynamic lubrication contacts*, ECCOMAS Computational Fluid Dynamics Conference,.

Carvalho, M.S. and Scriven, L.E. (1997), "Deformable Roll Coating Flows: Steady State and Linear Perturbation Analysis", *Journal of Fluid Mechanics*, 339, pp. 143-72.

Cudworth, C.J. (1979), *Finite element solution of the elastohydrodynamic lubrication of a compliant surface in pure sliding*, 5th Leeds-Lyon Symp. on Tribology, Leeds.

Dowson, D. and Higginson, G.R. (1959), "A Numerical Solution to the Elastohydrodynamic Problem", *J. Mech. Eng. Sci.*, 1, pp. 6-15.

Dowson, D. (1962), "A Generalised Reynolds Equation for Fluid Film Lubrication", *International Journal of Mechanical Engineering Sciences*, 4, pp. 159-70.

Dowson, D. and Ehret, P. (1999), "Past, Present and Future Studies in Elastohydrodynamics", *Proc I Mech E (J)*, 213, pp. 317-33.

Greenwood, J.A. (1999), "Transverse Roughness in Elastohydrodynamic Lubrication", *Proc I Mech E (J)*, 213, pp. 383-96.

Gupta, P.K. (1976), "On the heavily loaded elastohydrodynamic contacts of layered solids", *Trans. ASME, J. Lubric. Tech.*, 98, pp. 367-74.

Hannah, M. (1951), "Contact stress and deformation in a thin elastic layer", *Quarterly Journal of Mechanics and Applied Maths*, 4, pp. 94-105.

Higgson, G.R. (1965–-1966), "The theoretical effects of elastic deformation of the bearing liner on journal bearing performance", *Proc. Instn. Mech. Engrs.*, 180, pp. 31-8.

Hooke, C.J. and O'Donoghue, J.P. (1972), "Elastohydrodynamic lubrication of soft, highly deformed contacts", *Proc. I. Mech. E., Journal of Mechanical Engineering Sciences*, 14, pp. 34-48.

Hooke, C.J. (1986), "The elastohydrodynamic lubrication of a cylinder on a elastomeric layer", *Wear*, p. 111.

Hooke, C.J. (1999), "The behaviour of low amplitude surface roughness under line contacts", *Proc. Instn Mech. Engrs, Part J, Journal of Engineering Tribology*, 213, pp. 275-86.

Jaffar, M.J. (1993), "Determination of surface deformation of a bonded elastic layer indented by a rigid cylinder using Chebyshev series method", *Wear*, 170, pp. 291-4.

Lim, C.H., Bohan, M.F.J., Claypole, T.C., Gethin, D.T. and Roylance, B.J. (1996), "A finite element investigation into a soft rolling contact supplied by a non-newtonian ink", *J. Phys. D: Appl. Phys*, 29, pp. 1894-903.

Lunde, L. and Tønder, K. (1997), "Numerical Simulation of the Effects of Three-Dimensional Roughness on Hydrodynamic Lubrication: Correlation Coefficients", *Trans ASME (F)*, 119, pp. 315-22.

MacPhee, J., Shieh, J. and Hamrock, B.J. (1992), "The Application of Elastohydrodynamic Lubrication Theory to the Prediction of Conditions Existing in Lithographic Printing Press Roller Nips", *Advances in Printing Science and Technology*, 21, pp. 242-76.

Meijer, P. (1968), "The contact problem of a rigid cylinder on an elastic layer", *Applied Scientific Research*, 18, pp. 353-83.

Miller, R.D.W. (1966), "Some effects of compressibility on the indentation of a thin elastic layer by a smooth rigid cylinder", *Applied Scientific Research*, 16, pp. 405-24.

Patir, N. and Cheng, H.S. (1978), "An Average Flow Model for Determining Effects of Three-Dimensional Roughness on Partial Hydrodynamic Lubrication", *Trans ASME (F)*, 100, pp. 12-17.